Gravitationally Driven Wicking for Enhanced Condensation Heat Transfer

Citation: Preston, Daniel J. et al. "Gravitationally Driven Wicking for Enhanced Condensation Heat Transfer." Langmuir 34, 15 (March 2018): 4658–4664 © 2018 American Chemical Society

As Published: http://dx.doi.org/10.1021/ACS.LANGMUIR.7B04203

Publisher: American Chemical Society (ACS)

Persistent URL: https://hdl.handle.net/1721.1/121263

Version: Author's final manuscript: final author's manuscript post peer review, without publisher's formatting or copy editing

LANGMUIR Article
Cite This: Langmuir XXXX, XXX, XXX–XXX
pubs.acs.org/Langmuir

Gravitationally Driven Wicking for Enhanced Condensation Heat Transfer

Daniel J. Preston,[†] Kyle L. Wilke,[†,§] Zhengmao Lu,[†,§] Samuel S. Cruz,[†] Yajing Zhao,[†] Laura L. Becerra,[‡] and Evelyn N. Wang*[,†]

[†]Department of Mechanical Engineering, Massachusetts Institute of Technology, 77 Massachusetts Avenue, Cambridge, Massachusetts 02139, United States

[‡]Shiley-Marcos School of Engineering, University of San Diego, San Diego, California 92110, United States

Supporting Information

ABSTRACT: Vapor condensation is routinely used as an effective means of transferring heat or separating fluids. Filmwise condensation is prevalent in typical industrial-scale systems, where the condensed fluid forms a thin liquid film due to the high surface energy associated with many industrial materials. Conversely, dropwise condensation, where the condensate forms discrete liquid droplets which grow, coalesce, and shed, results in an improvement in heat transfer performance of an order of magnitude compared to filmwise condensation. However, current state-of-the-art dropwise technology relies on functional hydrophobic coatings, for example, long chain fatty acids or polymers, which are often not robust and therefore undesirable in industrial conditions. In addition, low surface tension fluid condensates, such as hydrocarbons, pose a unique challenge because common hydrophobic condenser coatings used to shed water (with a surface tension of 73 mN/m) often do not repel fluids with lower surface tensions (<25 mN/m). We demonstrate a method to enhance condensation heat transfer using gravitationally driven flow through a porous metal wick, which takes advantage of the condensate's affinity to wet the surface and also eliminates the need for condensate-phobic coatings. The condensate-filled wick has a lower thermal resistance than the fluid film observed during filmwise condensation, resulting in an improved heat transfer coefficient of up to an order of magnitude and comparable to that observed during dropwise condensation. The improved heat transfer realized by this design presents the opportunity for significant energy savings in natural gas processing, thermal management, heating and cooling, and power generation.

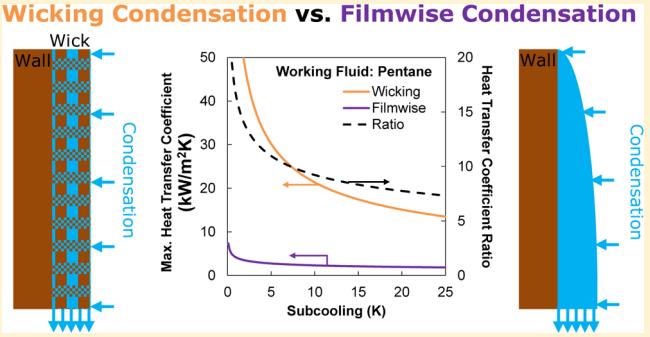

INTRODUCTION

Condensation is a ubiquitous phenomenon found throughout nature and implemented in many critical industrial applications for heat rejection and fluid processing. Filmwise condensation is prevalent in typical large-scale systems, where the condensed fluid forms a thin liquid film due to the high surface energy associated with many industrial materials.[1] Conversely, dropwise condensation, where the condensate forms discrete liquid droplets which grow, coalesce, and shed, results in an improvement in heat transfer performance of an order of magnitude compared to filmwise condensation.[2−6] During water condensation, the dropwise mode is often promoted with thin hydrophobic coatings.[6,7] However, low surface tension fluid condensates, such as hydrocarbons, pose a unique challenge because the typical hydrophobic condenser coatings used to shed water (surface tension $\gamma \approx 73$ mN/m) often do not repel fluids with lower surface tensions ($\gamma < 25$ mN/m). This is particularly relevant for natural gas processing[8,9] and refrigeration[10,11] applications. Reentrant and doubly reentrant surface designs have been proposed for repellency of low surface tension impinging droplets,[12,13] but these schemes are not useful during condensation when the impinging fluid can nucleate within the structures and subsequently render the surface hydrophilic.[14,15]

Compounding the issue of fluid repellency is the limited demonstration of effective, robust coatings in prior work. Thick polymer coatings are able to promote dropwise condensation for several years, but the added thermal resistance due to these coatings negates the improvement in heat transfer expected by transitioning to dropwise condensation.[16] Thin monolayer coatings effectively enhance condensation heat transfer, but typically fail within hours or days.[17] Recent work has suggested that alternative thin coatings, such as graphene applied by chemical vapor deposition (CVD)[5] or thin polymers applied by initiated CVD,[18] exhibit enhanced robustness, but accompanying experimental studies did not exceed 2 weeks in duration, leaving these methods uncertain pending more extensive characterization.

Received: December 11, 2017
Revised: March 23, 2018
Published: March 26, 2018

DOI: 10.1021/acs.langmuir.7b04203
Langmuir XXXX, XXX, XXX–XXX

In this work, we demonstrated an approach to enhance condensation heat transfer using gravitationally driven flow through a porous metal wick. This approach addresses the problems that traditional condenser surface coatings face by taking advantage of the attraction of the condensate to the bare metal surface and therefore avoiding the need for surface coatings altogether. We attach a high-thermal-conductivity metal wick to the condenser surface, which fills with condensate during operation. Because the thermal resistance of the combined wick−condensate composite is less than that of the film formed during filmwise condensation, condensation heat transfer is enhanced. We experimentally demonstrated a heat transfer enhancement of over 350% in this work. Furthermore, using an analytical model which was validated against the experimental data, we predicted that an enhancement of over an order of magnitude can be achieved with an optimized metal wick, potentially outperforming traditional dropwise condensation. This robust improvement in heat transfer presents an opportunity for long-term savings in many energy-intensive condensation applications.

■ ANALYSIS

We developed an analytical model to determine whether gravitationally driven wicking condensation would enhance heat transfer performance. This model, shown schematically in Figure 1, is conceptually similar to the Nusselt falling-film theory.[1] In Nusselt's theory, vapor at a uniform temperature (T_{vap}) condenses onto the fluid film surface, resulting in more fluid being added at the surface proportional to the local rate of heat transfer. The heat added by condensation at the surface is transferred through the fluid (or in the case of a gravitationally driven wicking condenser, the fluid and the wick) to the condenser wall, which is also at a uniform temperature (T_{wall}). The fluid added during condensation must then be removed by gravity. In Nusselt's theory, the fluid flows freely over the condenser surface constrained only by the no-slip condition at the condenser wall; in our case, flow through the wick can be modeled as flow in porous media. The heat transfer coefficient is found in Nusselt's theory by averaging the local conductance of the fluid film over the condenser surface; in our case, the same approach is followed, but in the case of a wick of uniform thickness filled with condensate, the local conductance is the same everywhere and is therefore equal to the average conductance. The condensation heat transfer coefficient for this special case of a wick with uniform thickness is calculated as

$$h_c = \frac{1}{R_c} = \frac{k_{wick}}{t} \quad (1)$$

where k_{wick} is the thermal conductivity of the combined wick−condensate composite and t is the thickness of the wick. If the thermal resistance of the wick is much lower than that of the fluid, then k_{wick} is approximately equal to the conductivity of the metal wick as measured under air or vacuum. From eq 1, we see that a thinner or more highly conductive wick will translate to a higher heat transfer coefficient.

In addition to calculating the heat transfer coefficient, we modeled the fluid flow inside the wick during condensation to determine the highest achievable subcooling before the gravitational pressure gradient becomes insufficient to drive fluid flow through the wick. This limiting case, referred to as "flooding" of the condenser, results in some of the fluid exiting the front surface of the wick and forming a falling fluid film on the surface of the combined wick−condensate composite, thereby degrading heat transfer performance. However, in contrast to the critical heat fluxes observed during flooding of dropwise condensation[19] (and more commonly encountered in the liquid-to-vapor phase change process of boiling[6,20,21]), flooding of a gravitationally driven wicking condenser is not catastrophic and instead manifests as a gradual decrease in heat transfer coefficient with increasing subcooling. Physically, as the subcooling passes the critical value at which gravity can no longer drive the flow of condensate through the wick, a thin film similar to the film in Nusselt's model begins to flow over the wick surface starting at the bottom (where the flow rate is the highest) and propagating upwards as subcooling is increased, thereby gradually adding an additional thermal resistance.

Because the heat transfer coefficient is uniform across the condenser surface prior to flooding, the heat flux and, correspondingly, the volumetric flux of condensate into the wick from the vapor are also uniform. This heat flux is calculated from the heat transfer coefficient determined in eq 1 and the subcooling, $\Delta T = T_{vap} - T_{wall}$, as $q'' = h_c \Delta T$. Then, the volumetric flux can be calculated from the heat flux using the latent heat of evaporation, h_{fg}, and the fluid density, ρ, as $\dot{V}''_{cond} = q''/\rho h_{fg}$. Condensation on the sides of the wick is neglected for $L/4t \gg 1$ in the case of a square or circular condenser face, where L is the condenser height, or if the sides of the wick are blocked by an impermeable material. Conservation of mass is then used to find the maximum volumetric flux flowing out the

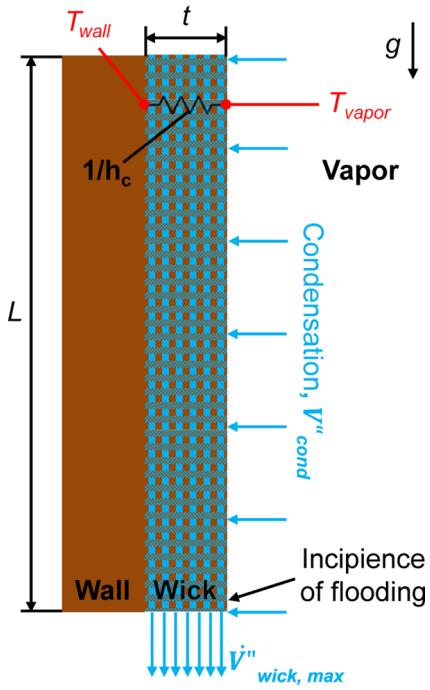

Figure 1. Schematic of the gravitationally driven wicking condenser design. Condensation, driven by the temperature drop from T_{vapor} to T_{wall} (the subcooling), occurs on the outermost surface of the wick, which is filled with condensate during operation. Gravity then drives the condensate downward toward the bottom of the wick, where it departs as a stream of droplets. Because the maximum condensate flow rate occurs at the bottom of the wick, flooding of the wick (which manifests as a thin condensate film on the surface of the wick) will first occur at the bottom and then propagate upwards under higher condensation rates.

DOI: 10.1021/acs.langmuir.7b04203
Langmuir XXXX, XXX, XXX−XXX

bottom surface of the wick, which is then used in Darcy's law for porous media flow

$$\dot{V}''_{\text{wick,max}} = \frac{\dot{V}''_{\text{cond}} L}{t} = \frac{\kappa}{\mu}\left|\frac{dP}{dx}\right|_{\text{max}} \quad (2)$$

where κ is the wick permeability, μ is the viscosity, and $|dP/dx|_{max}$ is the local pressure gradient required to drive flow at the point in the wick where the maximum volumetric flow rate occurs (the bottom of the wick). The required pressure gradient to drive fluid flow at each point in the wick is supplied only by the gravitational pressure gradient, ρg, so when these two pressure gradients are equal, we know that flooding is imminent. Setting the pressure gradients equal and substituting fundamental quantities from above yield

$$\left|\frac{dP}{dx}\right|_{\text{max}} = \frac{\Delta T L k_{\text{wick}} \mu}{\kappa \rho h_{\text{fg}} t^2} = \rho g \quad (3)$$

Equation 3 can be rearranged in terms of the subcooling, presented here as in inequality to indicate that subcooling values below the subcooling corresponding to the incipience of flooding are acceptable

$$\Delta T < \frac{\kappa \rho^2 g h_{\text{fg}} t^2}{L k_{\text{wick}} \mu} \quad (4)$$

This model is applicable to any condensate as long as the condensate fills the wick upon condensation as opposed to forming discrete droplets which depart from the wick surface; this latter case is only achievable for high intrinsic contact angles (significantly greater than 90°),[22] and does not apply to water or low surface tension fluids, such as hydrocarbons or refrigerants, on bare metal surfaces, even if these surfaces become contaminated by atmospheric volatile organic compounds.[23−26] For wicks with nonuniform height in the direction of gravity, for example, a circular condenser face as in the present work (Figure 2a), the longest dimension in the direction of gravity can be used to predict flooding because this dimension will correspond to the highest volumetric flux out of the bottom surface of the wick; for the wick attached to a circular condenser face, this is the diameter of the circle.

EXPERIMENT

Experiments were conducted in a controlled environmental chamber. The chamber allowed complete removal of noncondensable gases (NCGs) from the system (<1 Pa NCGs). Following removal of NCGs, pure, degassed vapor of the condensing fluid was introduced into the chamber from a heated, temperature-controlled canister and allowed to condense on the condenser surface. Operation of the environmental chamber is detailed in the Supporting Information. Pentane (Sigma-Aldrich, anhydrous, >99%) was chosen as the condensate for the experiments in the present work because it is a commonly used low surface tension fluid with applications in geothermal power production (as a working fluid),[27,28] natural gas processing (as a byproduct),[29,30] and as a blowing agent (where expended pentane can be recovered by condensation).[31−33] The results with pentane are representative of many low surface tension fluids, including hydrocarbons and chlorofluorocarbons, because these fluids typically have similar thermophysical properties, namely, low thermal conductivity and low latent heat compared to water.

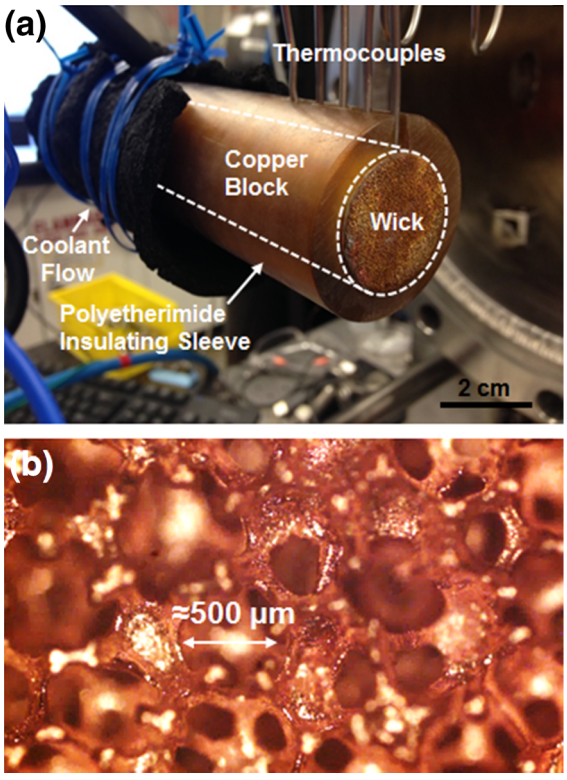

Figure 2. Experimental test fixture is shown in (a), where linear conduction in the copper block was used to calculate the heat flux and surface temperature, T_{wall}. The copper block was insulated by a polyetherimide sleeve (interface indicated with the white dashed lines) to prevent condensation on the sidewalls and generate a linear, one-dimensional temperature profile within the block. The experiment was conducted in a controlled environmental chamber, in which noncondensable gases (NCGs) were removed and the condensing fluid was introduced as vapor with a known temperature T_{vapor}. The copper wick was attached to the front of the copper block by diffusion bonding. A magnified view of the copper wick is shown in (b), where the characteristic pore size was approximately 500 μm.

The condenser wall temperature (T_{wall}) and heat flux (q'') were experimentally measured using a 1 in. diameter insulated copper block with thermocouples inserted into ports drilled along its length, shown in Figure 2a. The back end of the block was cooled with chiller water provided by an external chiller (Neslab, System I), and the front side of the block served as the condenser wall. From Fourier's law, the heat flux was obtained from the slope of the thermocouple temperature readings versus their location along the copper block. Similarly, the condenser wall temperature was determined by extrapolating this line to the condenser wall. The linear fit had an R^2 value of over 98% for each measurement, indicating that the assumption of linear conduction was valid and heat transfer through the block walls was negligible. The vapor pressure inside the chamber was measured (Omega, PX409-030A5V) and used to determine the vapor temperature (T_{vap}) from a saturation curve because both liquid and vapor were present inside the chamber. Then, the experimentally measured condensation heat transfer coefficient was determined by $h_{\text{c,exp}} = q''/\Delta T$. The uncertainty analysis is included in the Supporting Information Section S6.

We first experimentally characterized filmwise condensation of pentane on a flat copper condenser for comparison with Nusselt's falling-film theory to validate the experimental results. The flat copper condenser surface was fabricated by

DOI: 10.1021/acs.langmuir.7b04203
Langmuir XXXX, XXX, XXX−XXX

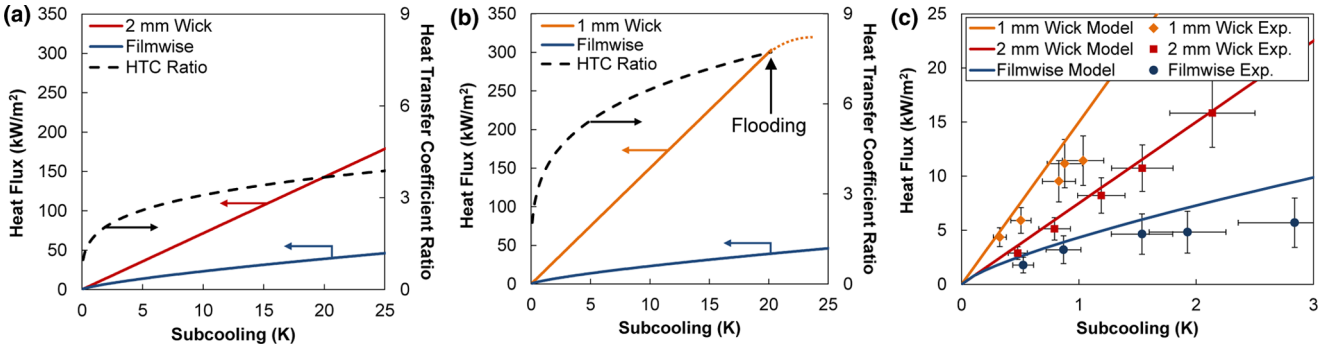

Figure 3. Modeling results for condensation of pentane on the copper wick (a) for a 2 mm thick wick and (b) for a 1 mm thick wick with the enhancement compared to filmwise condensation shown by the dashed black curve. The incipience of flooding, which is not catastrophic but rather a gradual decrease in heat transfer coefficient, is indicated in (b) (flooding occurs at a subcooling greater than 25 K in (a)). Experimental results are plotted with the model curves for the 1 mm and 2 mm thick wicks as well as for filmwise condensation in (c); the experimental results are in good agreement with the model prediction. Wicking condensation outperformed filmwise condensation by over 350% in the experimental analysis and is expected to achieve up to an order of magnitude enhancement at higher subcooling based on the modeling results.

mechanically and then chemically polishing the end of the copper block, solvent and acid cleaning the surface, and finally plasma cleaning with argon plasma. We then characterized condensation of pentane on both 2 mm and 1 mm thick copper foam wicks (copper foam wicks are common in heat exchangers and boiling phase change heat transfer applications[34−36] due to their robustness[37] and high thermal conductivity[37]). The copper foam, shown in Figure 2b, had a characteristic pore size of ≈500 μm, a porosity of 0.87, and a thermal conductivity of 14.7 W/(m K). The permeability of the wick was experimentally measured to be 1.25×10^{-9} m^2 (measurement described in Supporting Information Section S1). The copper foam was diffusion bonded to the copper block by first preparing the surface with the cleaning procedure used for the flat copper condenser, then inserting the copper foam and the copper block into a graphite holder (see Supporting Information Section S2), and finally performing the diffusion bond in a reducing tube furnace (Lindberg/Blue M) under the flow of forming gas (Airgas, 5% hydrogen, 95% nitrogen) at 800 °C for 1 h. The furnace temperature was achieved with a temperature ramp rate of 10 °C/min starting from ambient and then allowed to cool to 200 °C in the furnace before removal. The 2 mm thick copper foam bonded to the condenser wall is shown in Figure 2a.

RESULTS

Our analytical model was used to determine the expected heat flux versus subcooling for both the 2 mm and 1 mm thick copper foam wicks, shown in comparison to the expected heat flux during filmwise condensation in Figure 3a,b. The enhancement ratio of gravitationally driven wicking condensation compared to filmwise condensation is expected to exceed 4× and 8× for the 2 and 1 mm thick copper foam wicks, respectively, at high subcooling values. Additionally, the 1 mm thick wick would begin to flood at a subcooling of approximately 20 °C.

The experimental results were limited to a subcooling of less than 3 °C due to the cooling capacity of the chiller; therefore, flooding was not experimentally demonstrated in the present work, and the heat transfer coefficient was a constant value for each wick across the full range of experimental subcooling. Nonetheless, the heat fluxes were in excellent agreement with the predictions from the analytical model over the range of subcooling characterized experimentally, shown in Figure 3c. The experimentally demonstrated enhancements for the gravitationally driven wicking condensers were approximately 2−3× and 3−4× for the 2 mm and 1 mm thick copper foam wicks, respectively, in good agreement with the model prediction at these lower subcooling values. Furthermore, the agreement between Nusselt's model and the experimental results for filmwise condensation served to validate the experimental procedure. Note that Nusselt's prediction of heat transfer coefficient for a circular surface is only 5% greater than for a rectangular surface (see Supporting Information Section S3 for derivation); therefore, the more familiar solution for a rectangular surface was used to generate the model predictions shown in this work.

Following the successful comparison between prediction and experiment, we used the analytical model to determine the limitations of gravitationally driven wicking condensation. Given a condenser size, a condensing fluid, and a wick material, for each subcooling, an optimal wick thickness exists such that the heat transfer coefficient will be maximized. This thickness corresponds exactly to the incipience of flooding, because a thicker wick would have a lower heat transfer coefficient as calculated by eq 1, and a thinner wick would begin to flood and therefore also have a lower heat transfer coefficient. With this in mind, the maximum heat transfer coefficient that can be achieved by a gravitationally driven wicking condenser can be determined using this optimal thickness. One caveat, particularly at low subcooling, is that the optimal wick thickness may become so small that it approaches the characteristic length scale of the wick (in this case, the pore size). If the wick thickness is less than the characteristic length scale of the wick, the assumption that the wick−condensate composite is homogeneous is no longer valid, indicating that a wick with a smaller characteristic length scale should be used.

These values of maximum heat transfer coefficient are plotted as a function of subcooling for pentane as the condensate in Figure 4a; the nondimensional Nusselt number corresponding to the maximum heat transfer coefficient is included in the Supporting Information Section S10. The solid green lines indicate the performance of a wick that is either the optimal thickness or the characteristic length scale of the wick, whichever is larger; the dashed green lines indicate performance at the optimal wick thickness when this thickness is less than the characteristic length scale of the wick. If the desired subcooling for pentane condensation is known, the enhance-

DOI: 10.1021/acs.langmuir.7b04203
Langmuir XXXX, XXX, XXX−XXX

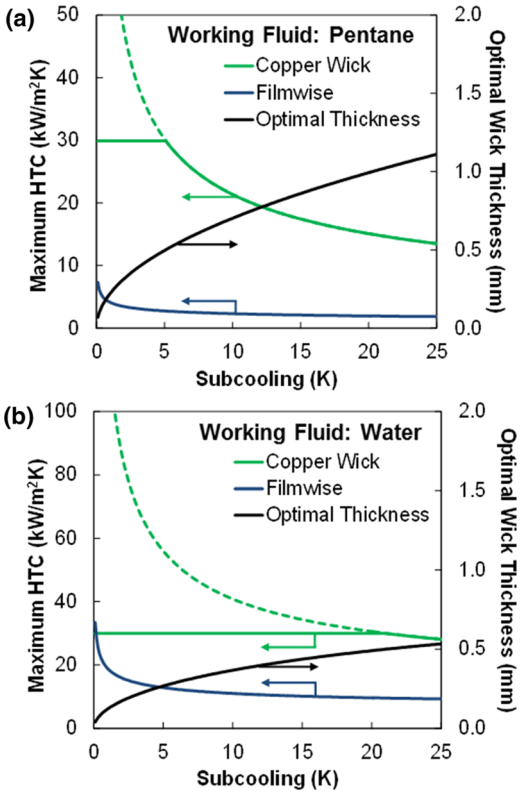

Figure 4. Maximum wick heat transfer coefficient, where the wick thickness is optimized for the highest possible heat transfer coefficient while also avoiding flooding at each value of subcooling, for the condensates (a) pentane and (b) water. The solid green lines indicate the performance of a wick that is either the optimal thickness or the characteristic length scale of the wick, whichever is larger; the dashed green lines indicate performance at the optimal wick thickness when this thickness is less than the characteristic length scale of the wick. The performance of pentane can be improved by over 5−10× compared to filmwise condensation, and the enhancement with water is expected to be approximately 3−5×. The difference in potential enhancement between these two fluids is primarily due to the higher filmwise condensation heat transfer coefficient of water, where the relatively high latent heat of water compared to pentane results in a thinner condensate film and correspondingly a lower thermal resistance; meanwhile, the heat transfer coefficient of wicking condensation remains virtually the same for different condensates because the wick itself is the primary path for thermal transport, as illustrated by the horizontal regions of the solid green curves where the wick thickness is constrained to the characteristic length scale of the wick.

ment using a gravitationally driven wicking condenser will be between 5× and 10× with the copper foam used in the present study applied at the optimal thickness, and with a condenser height L of 1 in., on the order of the height of many common industrial condensers.[11,38,39] Applying the model to water instead of pentane in Figure 4b, we show that the enhancement using gravitationally driven wicking condensation is up to 3× when constraining the wick thickness to be greater than the wick characteristic length scale. At lower subcooling values, greater enhancement is possible using a wick with a smaller characteristic length than the wick used in the present work, which could allow the performance indicated by the dashed green curve and a corresponding heat transfer enhancement of over 5× compared to filmwise condensation. This result suggests that wicking condensers are a viable alternative to dropwise condensation even for condensates for which hydrophobic coatings may be effective such as water.

DISCUSSION

Prior work has incorporated porous media and porous surfaces in condensation applications with the goal of enhancing heat transfer.[40−47] For example, porous fins have been added to the outside of a tube condenser to enhance condensation heat transfer of refrigerants by 180%.[48] Perhaps more similar to the present work, two experimental studies have applied a porous medium directly onto a condenser surface and reported heat transfer enhancements of 56%[49] and subsequently 200%[50] compared to filmwise condensation. Unfortunately, these reports did not demonstrate a clear understanding of the potential benefits of gravitationally driven wicking condensation; in fact, they designed systems in which condensate flowed over the top of the porous media, which corresponds to the nonoptimal flooded case described here that we specifically designed our condenser coatings to avoid.[49−52] By developing an accurate analytical model and using it to guide design choices, we were able to experimentally demonstrate an enhancement of over 350% with condensate flowing only through the porous medium (and not over its surface, which would have resulted in an added thermal resistance). In addition, the physical understanding presented in this work will allow optimization of future iterations of gravitationally driven wicking condensers.

Nonuniform wick thickness is a clear direction for future exploration in this area. For example, a wick that is thinner at the top to promote higher heat transfer but thicker at the bottom where fluid volumetric flow rate is higher to prevent flooding could result in significant improvements over the present work. In fact, the shape of an optimal wick thickness profile as a function of vertical distance along the condenser wall could be determined. Other future directions might be designing the wick internal geometry to tailor interface shape and increase effective condensation area[53] or decoupling the viscous loss for lateral flow along the condenser wall with the heat transfer enhancement gained in the direction perpendicular to the wall[54] and drawing concepts from studies in evaporation.[55,56] Detailed modeling of the flooded case might prove to be useful in some applications and could be another future direction. Finally, perhaps the most effective research area stemming from this work will be the application of hydrophobic coatings, meshes, or membranes to the uppermost surface of the wick to take advantage of capillary pressure in addition to the gravitational pressure gradient.

CONCLUSIONS

Current state-of-the-art dropwise condensation relies on functional hydrophobic coatings that are often not robust and additionally are not able to repel low surface tension fluid condensates such as hydrocarbons and refrigerants. We proposed an alternative approach, gravitationally driven wicking condensation, which takes advantage of the condensate's affinity to wet the surface and also eliminates the need for condensate-phobic coatings. The condensate-filled wick has a lower thermal resistance than the fluid film observed during filmwise condensation, resulting in an improved heat transfer coefficient of up to an order of magnitude and comparable to that observed during dropwise condensation. We experimentally demonstrated a heat transfer enhancement of over 350%

DOI: 10.1021/acs.langmuir.7b04203
Langmuir XXXX, XXX, XXX−XXX

with a copper foam wick. Furthermore, using an analytical model which was validated against the experimental data, we showed that an enhancement of over an order of magnitude can be achieved with an optimized metal wick, potentially outperforming traditional dropwise condensation. This robust improvement in heat transfer presents the opportunity for long-term energy savings in fluid separation, thermal management, heating and cooling, and power generation.

■ ASSOCIATED CONTENT

Supporting Information

The Supporting Information is available free of charge on the ACS Publications website at DOI: 10.1021/acs.langmuir.7b04203.

Measurement of wick characteristics, detailed procedure to attach wick to condenser surface, comparison of square versus circular condenser geometry during filmwise condensation, description of experimental setup and condensation procedure, error analysis, thermal profile analysis within condenser block, and capillary pressure and wettability considerations (PDF)

■ AUTHOR INFORMATION

Corresponding Author

*E-mail: enwang@mit.edu.

ORCID

Daniel J. Preston: 0000-0002-0096-0285

Zhengmao Lu: 0000-0002-5938-717X

Author Contributions

§K.L.W. and Z.L. contributed equally to this work.

Author Contributions

D.J.P. and E.N.W. conceived the idea. D.J.P. developed the model. All authors contributed to the experimental analysis. E.N.W. guided the work.

Notes

The authors declare no competing financial interest.

■ ACKNOWLEDGMENTS

We gratefully acknowledge funding support from the Abu Dhabi National Oil Company (ADNOC) with Dr. Abdullah Al Mahri as program manager and from the Office of Naval Research (ONR) with Dr. Mark Spector as program manager. D.J.P. acknowledges funding received by the National Science Foundation Graduate Research Fellowship under Grant No. 1122374. Any opinions, findings, conclusions, or recommendations expressed in this material are those of the authors(s) and do not necessarily reflect the views of the National Science Foundation. Z.L. acknowledges funding from the Air Force Office of Scientific Research (AFOSR) with Dr. Ali Sayir as program manager. This work was performed in part at the Center for Nanoscale Systems (CNS), a member of the National Nanotechnology Infrastructure Network (NNIN), which is supported by the National Science Foundation under NSF award no. ECS-0335765. CNS is part of Harvard University.

■ REFERENCES

(1) Nusselt, W. The surface condensation of steam. *Z. Ver. Dtsch. Ing.* **1916**, *60*, 569−575.

(2) Rose, J. W. Dropwise Condensation Theory. *Int. J. Heat Mass Transfer* **1981**, *24*, 191−194.

(3) Rose, J. W. On Mechanism of Dropwise Condensation. *Int. J. Heat Mass Transfer* **1967**, *10*, 755−762.

(4) Schmidt, E.; Schurig, W.; Sellschopp, W. Condensation of water vapour in film- and drop form. *Z. Ver. Dtsch. Ing.* **1930**, *74*, 544.

(5) Preston, D. J.; Mafra, D. L.; Miljkovic, N.; Kong, J.; Wang, E. N. Scalable graphene coatings for enhanced condensation heat transfer. *Nano Lett.* **2015**, *15*, 2902−2909.

(6) Cho, H. J.; Preston, D. J.; Zhu, Y.; Wang, E. N. Nanoengineering materials for liquid-vapour phase-change heat transfer. *Nat. Mater. Rev.* **2016**, *2*, No. 16092.

(7) Ma, X. H.; Rose, J. W.; Xu, D. Q.; Lin, J. F.; Wang, B. X. Advances in dropwise condensation heat transfer: Chinese research. *Chem. Eng. J.* **2000**, *78*, 87−93.

(8) Rufford, T. E.; Smart, S.; Watson, G. C. Y.; Graham, B. F.; Boxall, J.; da Costa, J. C. D.; May, E. F. The removal of CO2 and N-2 from natural gas: A review of conventional and emerging process technologies. *J. Pet. Sci. Eng.* **2012**, *94−95*, 123−154.

(9) Seader, J. D.; Henley, E. J. *Separation Process Principles*, 2nd ed.; Wiley: Hoboken, NJ, 2005; p 756.

(10) Vadgama, B.; Harris, D. K. Measurements of the contact angle between R134a and both aluminum and copper surfaces. *Exp. Therm. Fluid Sci.* **2007**, *31*, 979−984.

(11) Tanasawa, I. *Recent Advances in Condensation Heat Transfer*, In Proceedings of 10th International Heat Transfer Conference; Institute of Chemical Engineering, 1994; Vol. 2, pp 297−312.

(12) Liu, T. L.; Kim, C. J. C. Turning a surface superrepellent even to completely wetting liquids. *Science* **2014**, *346*, 1096−1100.

(13) Weisensee, P. B.; Torrealba, E. J.; Raleigh, M.; Jacobi, A. M.; King, W. P. Hydrophobic and oleophobic re-entrant steel microstructures fabricated using micro electrical discharge machining. *J. Micromech. Microeng.* **2014**, *24*, No. 095020.

(14) Varanasi, K. K.; Hsu, M.; Bhate, N.; Yang, W. S.; Deng, T. Spatial Control in the Heterogeneous Nucleation of Water. *Appl. Phys. Lett.* **2009**, *95*, No. 094101.

(15) Enright, R.; Miljkovic, N.; Al-Obeidi, A.; Thompson, C. V.; Wang, E. N. Condensation on Superhydrophobic Surfaces: The Role of Local Energy Barriers and Structure Length Scale. *Langmuir* **2012**, *28*, 14424−14432.

(16) Rose, J. W. Dropwise condensation theory and experiment: a review. *Proc. Inst. Mech. Eng., Part A* **2002**, *216*, 115−128.

(17) Miljkovic, N.; Preston, D. J.; Wang, E. N. Recent Developments in Altered Wettability for Enhancing Condensation. In *Encyclopedia of Two-Phase Heat Transfer and Flow II: Special Topics and Applications*; Thome, J. R., Kim, J., Eds.; World Scientific, 2015; pp 85−131.

(18) Paxson, A. T.; Yague, J. L.; Gleason, K. K.; Varanasi, K. K. Stable Dropwise Condensation for Enhancing Heat Transfer via the Initiated Chemical Vapor Deposition (iCVD) of Grafted Polymer Films. *Adv. Mater.* **2014**, *26*, 418−423.

(19) Haraguchi, T.; Shimada, R.; Kumagai, S.; Takeyama, T. The Effect of Polyvinylidene Chloride Coating Thickness on Promotion of Dropwise Steam Condensation. *Int. J. Heat Mass Transfer* **1991**, *34*, 3047−3054.

(20) Rahman, M. M.; Olceroglu, E.; McCarthy, M. Role of Wickability on the Critical Heat Flux of Structured Superhydrophilic Surfaces. *Langmuir* **2014**, *30*, 11225−11234.

(21) Carey, V. P. *Liquid-Vapor Phase-Change Phenomena: An Introduction to the Thermophysics of Vaporization and Condensation Processes in Heat Transfer Equipment*, 2nd ed.; Taylor and Francis: New York, 2008; p 742.

(22) Aili, A.; Li, H. X.; Alhosani, M. H.; Zhang, T. J. In *Characteristics of Jumping Droplet-Enhanced Condensation on Nanostructured Micromesh Surface*, Proceedings of the ASME 5th International Conference on Micro/Nanoscale Heat and Mass Transfer, 2016; Vol. 1.

(23) Takeda, S.; Fukawa, M.; Hayashi, Y.; Matsumoto, K. Surface OH group governing adsorption properties of metal oxide films. *Thin Solid Films* **1999**, *339*, 220−224.

(24) Schrader, M. E. Ultrahigh-Vacuum Techniques in Measurement of Contact Angles .3. Water on Copper and Silver. *J. Phys. Chem.* **1974**, *78*, 87−89.

DOI: 10.1021/acs.langmuir.7b04203
Langmuir XXXX, XXX, XXX−XXX

(25) Preston, D. J.; Miljkovic, N.; Sack, J.; Enright, R.; Queeney, J.; Wang, E. N. Effect of hydrocarbon adsorption on the wettability of rare earth oxide ceramics. *Appl. Phys. Lett.* **2014**, *105*, No. 011601.
(26) Schrader, M. E. Wettability of Clean Metal-Surfaces. *J. Colloid Interface Sci.* **1984**, *100*, 372−380.
(27) Hettiarachchia, H. D. M.; Golubovica, M.; Worek, W. M.; Ikegami, Y. Optimum design criteria for an Organic Rankine cycle using low-temperature geothermal heat sources. *Energy* **2007**, *32*, 1698−1706.
(28) Franco, A.; Villani, M. Optimal design of binary cycle power plants for water-dominated, medium-temperature geothermal fields. *Geothermics* **2009**, *38*, 379−391.
(29) Sutton, R. P. Fundamental PVT calculations for associated and gas/condensate natural-gas systems. *SPE Reservoir Eval. Eng.* **2007**, *10*, 270−284.
(30) Gulsby, J. G. Low Temperature Process for Separating Propane and Heavier Hydrocarbons from a Natural Gas Stream. U.S. Patent 4,251,249, 1981.
(31) Burt, J. G.; Franklin, B. M. Method and Apparatus for Recovering Blowing Agent in Foam Production. U.S. Patent 4,531,951, 1985.
(32) Johnson, R. W. The effect of blowing agent choice on energy use and global warming impact of a refrigerator. *Int. J. Refrig.* **2004**, *27*, 794−799.
(33) Harvey, L. D. D. Net climatic impact of solid foam insulation produced with halocarbon and non-halocarbon blowing agents. *Build. Sci.* **2007**, *42*, 2860−2879.
(34) Xu, J.; Ji, X. B.; Zhang, W.; Liu, G. H. Pool boiling heat transfer of ultra-light copper foam with open cells. *Int. J. Multiphase Flow* **2008**, *34*, 1008−1022.
(35) Choon, N. K.; Chakraborty, A.; Aye, S. M.; Wang, X. L. New pool boiling data for water with copper-foam metal at sub-atmospheric pressures: Experiments, and correlation. *Appl. Therm. Eng.* **2006**, *26*, 1286−1290.
(36) Yang, Y.; Ji, X. B.; Xu, J. L. Pool boiling heat transfer on copper foam covers with water as working fluid. *Int. J. Therm. Sci.* **2010**, *49*, 1227−1237.
(37) Davies, G. J.; Zhen, S. Metallic Foams-Their Production, Properties and Applications. *J. Mater. Sci.* **1983**, *18*, 1899−1911.
(38) Salam, B.; McNeil, D. A.; Burnside, B. M. Pressure drop measurements in a low pressure steam condenser with a horizontal bundle of staggered tubes. *Appl. Therm. Eng.* **2004**, *24*, 1365−1379.
(39) Kim, S. J.; No, H. C. Turbulent film condensation of high pressure steam in a vertical tube. *Int. J. Heat Mass Transfer* **2000**, *43*, 4031−4042.
(40) Jain, K. C.; Bankoff, S. G. Laminar Film Condensation on a Porous Vertical Wall With Uniform Suction Velocity. *J. Heat Transfer* **1964**, *86*, 481−489.
(41) Cheng, P. Film Condensation Along an Inclined Surface in a Porous-Medium. *Int. J. Heat Mass Transfer* **1981**, *24*, 983−990.
(42) Cheng, P.; Chui, D. K. Transient Film Condensation on a Vertical Surface in a Porous-Medium. *Int. J. Heat Mass Transfer* **1984**, *27*, 795−798.
(43) Majumdar, A.; Tien, C. L. Effects of Surface-Tension on Film Condensation in a Porous-Medium. *J. Heat Transfer* **1990**, *112*, 751−757.
(44) Al-Nimr, M. A.; AlKam, M. K. Film condensation on a vertical plate imbedded in a porous medium. *Appl. Energy* **1997**, *56*, 47−57.
(45) Chang, T. B.; Yeh, W. Y. Effects of uniform suction and surface tension on laminar filmwise condensation on a horizontal elliptical tube in a porous medium. *Int. J. Therm. Sci.* **2009**, *48*, 2323−2330.
(46) Sanya, A. S. O.; Akowanou, C.; Sanya, E. A.; Degan, G. Liquid film condensation along a vertical surface in a thin porous medium with large anisotropic permeability. *SpringerPlus* **2014**, *3*, 659.
(47) Degan, G.; Sanya, A.; Akowanou, C. Laminar film condensation along a vertical plate embedded in an anisotropic porous medium with oblique principal axes. *Heat Mass Transfer* **2016**, *52*, 2119−2128.
(48) Shekarriz, A.; Plumb, O. A. Enhancement of Film Condensation Using Porous Fins. *J. Thermophys. Heat Transfer* **1989**, *3*, 309−314.
(49) Renken, K. J.; Aboye, M. Experiments on Film Condensation Promotion within Thin Inclined Porous Coatings. *Int. J. Heat Mass Transfer* **1993**, *36*, 1347−1355.
(50) Renken, K. J.; Mueller, C. D. Measurements of Enhanced Film Condensation Utilizing a Porous Metallic Coating. *J. Thermophys. Heat Transfer* **1993**, *7*, 148−152.
(51) Renken, K. J.; Soltykiewicz, D. J.; Poulikakos, D. A Study of Laminar-Film Condensation on a Vertical Surface with a Porous Coating. *Int. Commun. Heat Mass Transfer* **1989**, *16*, 181−192.
(52) Renken, K. J.; Aboye, M. Analysis of Film Condensation within Inclined Thin Porous-Layer Coated Surfaces. *Int. J. Heat Fluid Flow* **1993**, *14*, 48−53.
(53) Lu, Z.; Preston, D. J.; Antao, D. S.; Zhu, Y.; Wang, E. N. Coexistence of pinning and moving on a contact line. *Langmuir* **2017**, *33*, 8970−8975.
(54) Hanks, D. F.; Lu, Z.; Sircar, J.; Antao, D.; Barabadi, B.; Salamon, T.; Simon, E.; Enright, R.; Wang, E. N. *Evaporation Device with Nanoporous Membrane*, In International Electronic Packaging Technical Conference and Exhibition, San Francisco, CA, July 6−9, 2015.
(55) Wilke, K. L.; Barabadi, B.; Zhang, T. J.; Wang, E. N. Controlled Wetting in Nanoporous Membranes for Thin Film Evaporation. *J. Heat Transfer* **2016**, *138*, No. 080906.
(56) Lu, Z.; Wilke, K. L.; Preston, D. J.; Kinefuchi, I.; Chang-Davidson, E.; Wang, E. N. An Ultrathin Nanoporous Membrane Evaporator. *Nano Lett.* **2017**, *17*, 6217−6220.

DOI: 10.1021/acs.langmuir.7b04203
Langmuir XXXX, XXX, XXX−XXX

Supporting Information for:

Gravitationally Driven Wicking for Enhanced Condensation Heat Transfer

Daniel J. Preston[1], Kyle L. Wilke[1, †], Zhengmao Lu[1, †], Samuel S. Cruz[1], Yajing Zhao[1], Laura L. Becerra[2], Evelyn N. Wang[1,*]

[1]*Department of Mechanical Engineering, Massachusetts Institute of Technology, 77 Massachusetts Ave., Cambridge, MA 02139, USA*

[1]*Shiley-Marcos School of Engineering, University of San Diego, San Diego, CA 92110, USA*

† Equal contribution

**Corresponding author email: enwang@mit.edu*

S1. Permeability Measurement

The wicking properties were determined by measuring the propagation of fluid through the wicking sample as a function of time following a well-known procedure.[1] The test apparatus was comprised of a stationary copper foam sample and a fluid reservoir which was filled with deionized water, shown in Figure S1. Prior to the experiment, a rectangular copper foam sample was first solvent cleaned with acetone, ethanol, and isopropanol, then treated with 0.2 M hydrochloric acid in water for 1 minute, dried with a clean nitrogen stream, and finally plasma cleaned with argon plasma for 30 minutes, at which point the contact angle on copper was approximately zero degrees, in agreement with past work.[2] The sample was immediately mounted on the clip, and the water reservoir was raised slowly (less than 0.1 mm/sec) until contact was made with the sample, at which point the wicking process was observed with a high speed camera (Vision Research Phantom 7.1). The propagation of the liquid front was quantified by post-processing the high speed videos using imaging analysis software.

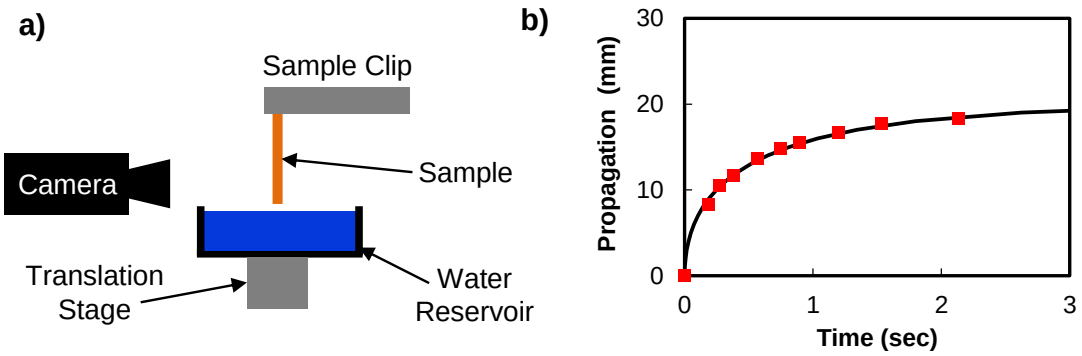

Figure S1. (a) Experimental setup for permeability characterization and (b) experimentally-measured fluid propagation distance for water used to determine the wick permeability. Red data points in (b) are experimental data, and the black curve is the model solution generated by Equation S2 fit to the experimental data to determine the permeability.

To determine the permeability from the experimental data, we modeled the fluid propagation with the one-dimensional Darcy's law with gravitational effects included to account for liquid propagation against gravity over a distance greater than the capillary length:

$$\frac{dy}{dt} = \frac{-\kappa}{\mu\varphi}\left(\frac{-\Delta P_{cap}}{y} - \rho g\right) \tag{S1}$$

where the derivative of the propagation distance, y, with respect to time, t, is shown as a function of the viscosity (μ) and density (ρ) of the propagating fluid as well as the gravitational acceleration (g) and wick property of porosity (φ), determined from comparing the wick's bulk and apparent densities. The driving capillary pressure (ΔP_{cap}) and permeability of the wick (κ) were determined from fitting the model solution to the experimental data (Figure S2(b), black curve). The solution can be found explicitly for time as a function of the distance over which the fluid has propagated (solving for propagation distance as a function of time requires implementation of the Lambert W function and is not presented here):

$$t = \frac{Aln(A - By) + By - Aln(A)}{(B)^2}, \qquad A = \frac{\kappa \Delta P_{cap}}{\mu \varphi}, \qquad B = \frac{\kappa \rho g}{\mu \varphi} \tag{S2}$$

Therefore, from the physical parameters μ, ρ, φ, g, and the experimental fluid propagation data, the capillary pressure and permeability can be determined for any given wicking material (shown in Table S1 below for copper foam). Note that the permeability is a geometric parameter that does not change when modeling different fluids; the capillary pressure does change from fluid to fluid, but if all of the fluids considered have the same contact angle (e.g., zero degrees), then the ratio of capillary pressure for two different fluids within a wick is equivalent to the ratio of their surface tensions.

Table S1. Experimentally-determined capillary pressure (water) and permeability for copper foam wick.

Sample (density)	**Char. Dimension**	**Permeability**	**Cap. Pressure**
Cu Foam Wick (1,165 kg/m^3)	500 μm	1.25 x 10^{-9} m^2	0.2 kPa

S2. Bonding Wick to Condenser Surface

In order to obtain good thermal contact between the copper condenser block and the copper foam, we diffusion-bonded the copper foam to the block. First, we machined a graphite fixture on the lathe to hold the copper block, shown schematically in Figure S2(a). The copper block was pressed against the copper foam, shown in Figure S2(b), and placed inside of a furnace (Lindberg/Blue M tube furnace). The furnace was purged and kept under forming gas (Airgas, 5% hydrogen, 95% nitrogen) throughout the bonding procedure. The furnace was heated from room temperature to 800 °C at a ramp rate of 10 °C/min and maintained at 800 °C for 1 hour, then allowed to cool to 200 °C over the course of 3 hours. The diffusion-bonded copper wick on the copper condenser block is shown in Figure S2(c).

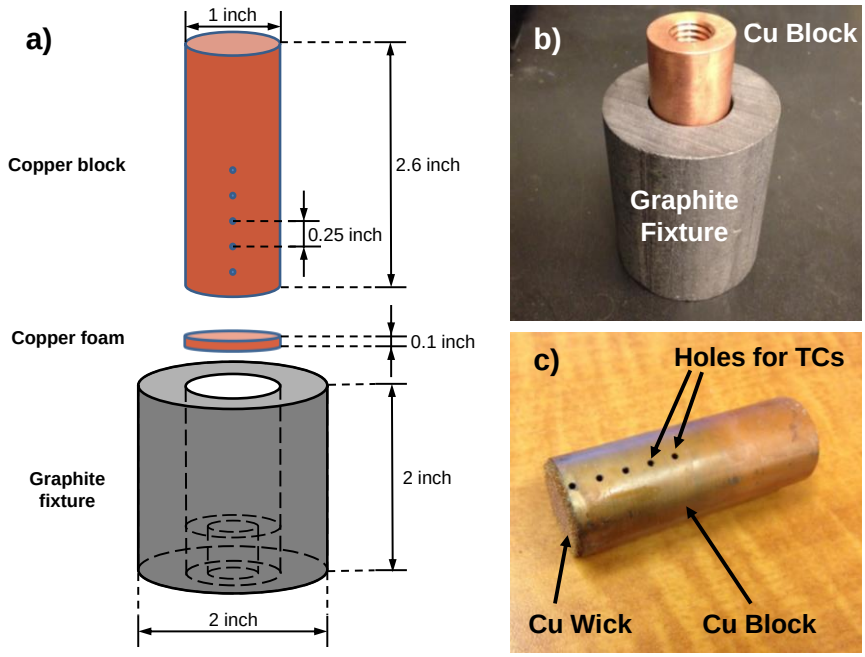

Figure S2. A graphite fixture was machined to hold the copper block as shown schematically in (a) with dimensions of the copper block, the copper foam, and the graphite fixture detailed. The copper foam was attached to the copper block by diffusion bonding in a furnace; the graphite fixture kept the wick aligned to the condenser surface (b). The final diffusion-bonded wick on copper test fixture is shown in (c).

S3. Nusselt Model: Comparison of Circular to Rectangular Condenser Wall

To model filmwise condensation on a smooth condenser surface with a uniform height L, the Nusselt model is applied:[3]

$$h_{c,Nu} = 0.943\left(\frac{g\rho_c(\rho_c - \rho_v){k_c}^3 h'_{fg}}{\mu L \Delta T}\right)^{1/4} \quad \text{(S3)}$$

$$h'_{fg} = h_{fg} + 0.68c_{p,l}\Delta T \quad \text{(S4)}$$

where g is the gravitational acceleration (g = 9.81 m/s^2), ρ_v is the vapor density, ρ_c is the liquid condensate density, μ is the condensate dynamic viscosity, k_c is the condensate thermal conductivity, ΔT is the temperature difference from the surrounding vapor to the condenser wall, h'_{fg} is the modified latent heat of vaporization accounting for the change in specific heat of the condensate, and $c_{p,l}$ is the condensate specific heat.[3]

Since the experiments in the present work were conducted on a circular condenser surface, i.e., a surface with a nonuniform height, we adjusted the Nusselt model for this scenario to determine whether the results would be significantly different than those for a condenser with uniform height. This analysis was performed by treating the circular surface as a series of infinitesimally thin vertical strips with width dx, applying Nusselt's model to each strip, and then integrating laterally across the surface to find the average heat transfer coefficient for the entire surface. If the horizontal x-coordinate is zero at the center of the circular surface and the diameter of the circle is *L*, the height of each vertical strip is:

$$H = 2\sqrt{(L/2)^2 - x^2} \tag{S5}$$

Then, the heat transfer coefficient of each vertical strip is:

$$h_{c,x} = 0.943\left(\frac{g\rho_c(\rho_c - \rho_v){k_w}^3 {h'}_{fg}}{\mu_c H \Delta T}\right)^{1/4} \tag{S6}$$

Integrating the area-weighted heat transfer coefficient, $h_{c,x}Hdx$, from –L/2 to L/2 and dividing by the surface area (which is fundamentally the same procedure as adding thermal resistances in parallel),

$$h_{c,circle} = \frac{4}{\pi L^2}\int_{-L/2}^{L/2} h_{c,x} H dx \tag{S7}$$

yields:

$$h_{c,circle} = \frac{6\Gamma(3/8)}{7\sqrt{\pi}\Gamma(7/8)} h_{c,Nu} = 1.052\, h_{c,Nu} \tag{S8}$$

where Γ is the gamma function. This result shows that the heat transfer coefficient for filmwise condensation on a circular surface for a circle of diameter *L* is only ≈ 5% greater than on a surface with uniform height *L*. We neglected this small difference in favor of the more familiar Nusselt model for a condenser surface with uniform height, which is used throughout the analysis in the main text.

S4. Environmental Chamber Setup

The custom environmental chamber used for this work consists of a stainless steel frame with a door (sealed with a rubber gasket), two viewing windows, and apertures for various components. Resistive heater lines were wrapped around the exterior of the chamber walls to prevent condensation at the inside

walls and then insulated on the exterior walls. The output power of the resistive heater lines was controlled by a voltage regulator. Two insulated stainless steel water flow lines (Swagelok) were fed into the chamber to supply cooling water to the chamber from a large capacity chiller.

An additional stainless steel tube line was fed into the chamber that served as the flow line for the incoming vapor supplied from a heated stainless steel reservoir. The vapor line was wrapped with a rope heater (60 W, Omega) controlled by a power supply. The vapor reservoir was wrapped with another independently-controlled heater (120 W, Omega) and insulated to limit heat losses to the environment. The access tubes were welded to the vapor reservoir, each with independently-controlled valves. The first valve (Diaphragm Type, Swagelok), connecting the bottom of the reservoir to the ambient, was used to fill the reservoir with the working fluid to be condensed. The second valve (BK-60, Swagelok), connecting the top of the reservoir to the inside of the chamber, provided a path for vapor inflow. T-type thermocouples were located along the length of the water vapor reservoir to monitor temperature.

A bellows valve (Kurt J. Lesker) was attached to the chamber to serve as a leak port between the ambient and inside of the chamber. In order to monitor temperatures within the chamber, T-type thermocouple bundles were connected through the chamber apertures *via* a thermocouple feed through (Kurt J. Lesker). A pressure transducer (PX409-030A5V, Omega) was attached to monitor pressure within the chamber. The thermocouple bundles and the pressure transducer were both electrically connected to an analog input source (RAQ DAQ, National Instruments), which was interfaced to a computer for data recording. A second bellows valve (Kurt J. Lesker) was integrated onto the chamber for the vacuum pump, which brought the chamber to vacuum conditions prior to vapor filling. A liquid nitrogen cold trap was incorporated along the line from the chamber to the vacuum which served to remove any moisture from the pump-down process and ultimately assist in yielding higher quality vacuum conditions. A tertiary bellows valve (Kurt J. Lesker) was integrated on a T fitting between the vacuum pump and liquid nitrogen reservoir to connect the vacuum line to the ambient to release the vacuum line to ambient conditions once pump down was achieved.

S5. Fin Analysis of Condenser Block

To determine the condensation heat flux and condenser surface temperature, we recorded temperatures at evenly-spaced thermocouples mounted within the copper condenser block; we input these temperatures into the 1-dimensional form of Fourier's law to determine the heat flux, and, from a corresponding thermal resistance network for the copper block, the surface temperature was determined. The copper block was insulated with a polyetherimide sleeve to minimize heat transfer at the sidewalls, shown in

Figure 2 in the main text. In order to justify the use of the 1-dimensional Fourier's law in this case, we performed a fin analysis on the insulated copper condenser block, detailed in this section.

First, we calculated the Biot number for a cross-section of the insulated copper condenser block. Heat conduction occurred along the axis of the cylindrical block, so the appropriate cross-section for the Biot number analysis was a circular cross-section of the cylindrical block and the insulating sleeve. The cylindrical copper block has a diameter of D = 1 inch (≈ 0.0254 m), and the polyetherimide insulating sleeve has a wall thickness of t_{ins} = 0.25 inches (≈ 0.0064 m). We used the thermal conductivity of copper (k_{Cu} = 400 W/m-K) and the radius of the cylindrical copper block to calculate the Biot number; the characteristic heat transfer coefficient for the sidewall of the block was obtained by adding the heat transfer coefficient for condensation (conservatively taken as h_c = 10,000 W/m^{2}K in the present work) on the outer surface of the insulation with the thermal admittance of the insulation itself (with a thermal conductivity of k_{ins} = 0.22 W/m-k for polyetherimide) in series, as shown in Equation S9:

$$h_{wall} = \left(\frac{1}{h_{cond}} + \frac{t_{ins}}{k_{ins}}\right)^{-1} = \left(\frac{1}{10{,}000\ W/m^2 \cdot K} + \frac{0.0064\ m}{0.22\ W/m \cdot K}\right)^{-1} = 34\ W/m^2 \cdot K \qquad \text{(S9)}$$

The insulation was treated as a thin sheet; if it were treated as an annulus, the results of this section would not change significantly. The Biot number is calculated in Equation S10:

$$Bi = \frac{h_{wall}(D/2)}{k_{Cu}} = \frac{34\ W/m^2 \cdot K\ ((0.0254\ m)/2)}{400\ W/m \cdot K} = 0.001 \ll 1 \qquad \text{(S10)}$$

Since the Biot number for the condenser block cross-section is much less than unity, each cross section is approximately isothermal and the block can be treated as a fin. The heat equation simplified for a cylindrical fin at steady state is:

$$\frac{d^2T}{dx^2} = \frac{h_{wall}\pi D}{k_{Cu}(\pi/4)D^2}(T - T_\infty) \qquad \text{(S11)}$$

where T is the temperature at any point, x, along the length of the fin, and T_∞ is the temperature of the surroundings (in this case, the saturated vapor). Making the substitutions $\theta = T - T_\infty$ and $m^2 = (h_{wall}\pi D)/(k_{Cu}(\pi/4)D^2)$, the solution to the differential equation S11 is:

$$\theta(x) = C_1 e^{mx} + C_2 e^{-mx} \tag{S12}$$

The following boundary conditions were applied, representing: (S13) a set base temperature achieved by the coolant flow that cooled the block at (x = 0); and (S14) a heat flux set by the condensation heat transfer coefficient at the condenser surface (x = L) and the temperature difference from the condenser surface to the surrounding vapor, $\theta_L = T(x = L) - T_\infty$:

$$\theta_B = T_B - T_\infty \tag{S13}$$

$$h_{cond}\theta_L = -k_{Cu}\left.\frac{d\theta}{dx}\right|_{x=L} \tag{S14}$$

Application of these boundary conditions to Equation S12 results in the following constants:

$$C_1 = \theta_B \frac{\frac{-h_{cond}}{k_{Cu}} e^{-mL} + m e^{-mL}}{2m\cosh(mL) + 2\frac{h_{cond}}{k_{Cu}}\sinh(mL)} \tag{S15}$$

$$C_2 = \theta_B \left[1 - \frac{\frac{-h_{cond}}{k_{Cu}} e^{-mL} + m e^{-mL}}{2m\cosh(mL) + 2\frac{h_{cond}}{k_{Cu}}\sinh(mL)}\right] \tag{S16}$$

Equation S12, with the constants obtained from Equations S15 and S16, was used to determine the temperature profile within the cylindrical copper condenser block for a block length of 8 cm, a block base temperature (where it is cooled by chiller fluid) of T_B = 19 °C, and a surrounding vapor temperature of T_∞ = 22 °C, all characteristic of a typical experiment. The results are shown in Figure S3 below, where the region of the block into which the thermocouples were inserted exhibits a linear, one-dimensional temperature profile.

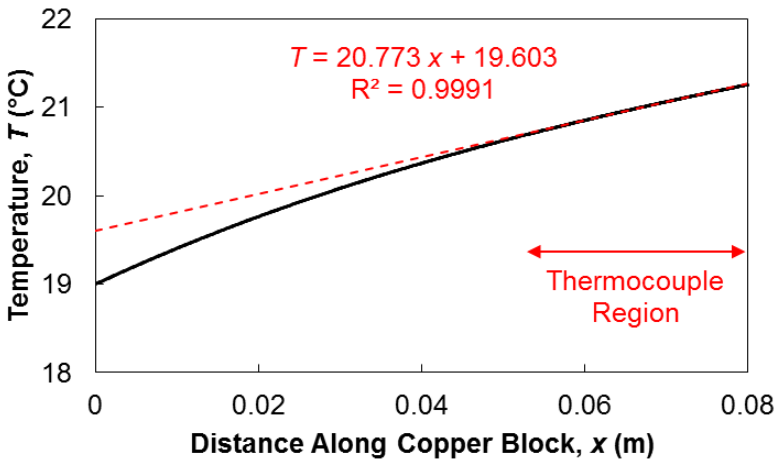

Figure S3. Results of the analytical fin model applied to the cylindrical copper condenser block used in the experiments in this work. The temperature profile over the region where the thermocouples were inserted into the copper block was approximately linear, with an R^2 value of 0.9991 for a linear fit (dashed red line) to the temperature profile (solid black line) within the thermocouple region.

S6. Condensation Procedure

For each experimental trial, a set of strict procedures was followed to ensure consistency throughout the experiments. The first step of the process was to turn on the voltage regulator to heat up the environmental chamber walls, which prevented condensation on the chamber walls. Simultaneously, the vapor reservoir was filled with approximately 2 liters of either DI water or pentane. After opening the vapor inflow valve and closing the liquid release valve, the rope heater around the vapor reservoir was turned on with the heater controller set to maximum output (120 W). Then the rope heater connected to the vapor inflow valve was turned on. The temperature of the reservoir was monitored with the installed thermocouples; the temperature at the top of the reservoir was higher than that of the middle/bottom of the reservoir due to the water thermal-mass present at the middle/bottom section. Hence, we ensured that the regions of the reservoir of higher thermal capacity were brought to a sufficiently high temperature for boiling. During the boiling process, aluminum foil was placed on the bottom surface of the inner chamber to collect any fluid leaving the vapor inflow line. Once boiling was achieved and the internal thermocouple on the reservoir was 5˚C above the boiling point for at least 10 minutes, the vapor inflow valve was closed. The excess fluid that spilled inside the chamber during de-gassing of the reservoir was removed.

In order to install the sample inside of the chamber, the rear end of the condenser block (the far-right side of the block in Figure S2(c)) was bolted on to a copper fixture chilled with cold water supplied from the external chiller. Before installing the entire sample setup in the chamber, all adapters/connecters were tightened to ensure that there were no leaks that could affect vacuum performance.

Next, we performed the vacuum pump-down procedure. Initially, the liquid nitrogen cold trap was filled to about half capacity. The ambient exposed valves connecting the chamber and the vacuum pump were both closed and the valve connected to the liquid nitrogen cold trap was opened. The vacuum pump was then turned on, initiating the pump-down process. The pressure inside the chamber was monitored during the pump-down process. This process took approximately one hour in order to achieve the target vacuum conditions (0.5 Pa < P < 1 Pa). The experimental operating pressure of non-condensable was set to be a maximum of 0.25% of the operating pressure. Non-condensable gas content of above 0.5% (pressure) has been shown to significantly degrade performance during dropwise condensation.[4] In our experiments, extreme care was taken to properly de-gas the vacuum chamber and water vapor reservoir prior to experimental testing. In addition, the chamber leak rate was characterized prior to each run in order to estimate the maximum time available for acquiring high fidelity data with non-condensable content of less than 0.25%.

The setup of the water flow-loop is described as follows: the water pump reservoir was filled and turned on to a flow rate of 8 L/min. The flow rate was monitored with a flow meter integrated in the inflow water line. In order to bring the chilled water into the flow loop and to the tube sample, the external chilled water lines were opened.

To begin experiments, the vapor inflow valve was slowly opened until the operating pressure was reached. Steady state conditions were typically reached after 2 minutes of full operation. Temperature measurements were recorded at evenly-spaced thermocouples mounted within the copper condenser block and input into the 1-dimensional Fourier's law to determine the heat flux; from a corresponding thermal resistance network for the copper block, the surface temperature is determined. With the vapor temperature already known, the heat flux can be plotted against the subcooling (vapor temperature minus the surface temperature of the copper condenser block).

S7. Heat Transfer Coefficient and Error Propagation

This section presents the method used for error analysis of the experimental results. The heat flux can be determined from the 1-dimensional Fourier's law as shown here:

$$q" = \frac{k_{block}(T_1 - T_5)}{d_{1-5}} \tag{S17}$$

where $q"$ is the overall condensation heat flux, T_1 and T_5 are the condenser block temperatures measured closed to and farthest from the surface, respectively, k_{block} is the thermal conductivity of the condenser block, and $d_{1\text{-}5}$ is the distance between thermocouples 1 and 5. The corresponding error in the experimentally determined heat flux can be calculated by propagating the error of each component based on the method of first partial derivatives:

$$E_{q"} = \sqrt{\left(\frac{k_{block}E_{T1}}{d_{1-5}}\right)^2 + \left(\frac{-k_{block}E_{T5}}{d_{1-5}}\right)^2 + \left(\frac{(T_1 - T_5)E_{k_{block}}}{d_{1-5}}\right)^2 + \left(\frac{-(T_1 - T_5)k_{block}E_{d_{1-5}}}{(d_{1-5})^2}\right)^2} \tag{S18}$$

where E represents the absolute error in each quantity. Similarly, based on 1-dimensional conduction, the subcooling, ΔT_{sub}, of the condenser block (the vapor temperature minus the surface temperature beneath the wick or fluid film for wicking or filmwise condensation, respectively) can be determined:

$$\Delta T_{sub} = T_{sat} - T_1 - \frac{q"d_{s-1}}{k_{block}} \tag{S19}$$

where T_{sat} is the saturation temperature of the surrounding vapor and $d_{s\text{-}1}$ is the distance between the thermocouple closest to the condenser block surface and the surface of the block. Again propagating the error of each component based on the method of first partial derivatives:

$$E_{\Delta T_{sub}} = \sqrt{(E_{Tsat})^2 + (-E_{T1})^2 + \left(\frac{-d_{s-1}E_{q"}}{k_{block}}\right)^2 + \left(\frac{-q"E_{d_{s-1}}}{k_{block}}\right)^2 + \left(\frac{q"d_{s-1}E_{k_{block}}}{(k_{block})^2}\right)^2} \tag{S20}$$

Table S2 below summarizes the uncertainty associated with each experimental measurement.

Table S2. Uncertainties corresponding to experimental measurements.

Experimental Measurement	Uncertainty
Calibrated thermocouple (T_1, T_5)	0.1 K
Saturated vapor pressure (P_v)	1%
Saturated vapor temperature (T_v)	$T_{sat}(1.01(P_v))$-$T_{sat}(P_v)$
Copper thermal conductivity (k_{block})	1%
Distance measurement ($d_{1\text{-}5}$, $d_{s\text{-}1}$)	0.5 mm

S8. Capillary Pressure Considerations

The wick capillary pressure for water was measured to be 200 Pa using the procedure described in Section S1 above. Correspondingly, assuming complete wetting of the copper foam by both water and pentane, the capillary pressure of pentane is equal to the capillary pressure of water multiplied by the ratio of the surface tension of pentane to that of water, which yields P_{cap} = 44 Pa. Then, the capillary rise of pentane in the wick when no condensation occurs is $h_0 = P_{cap}/(\rho g)$ = 7 mm; that is to say, when no condensation occurs, the wick is only filled with pentane up to a height of 7mm from its base. As the subcooling is increased incrementally from zero and condensation begins, the wick is still not completely full of condensate, but a thin layer of condensate must necessarily form within the wick. Therefore, at very low subcooling, it is possible that the average heat transfer coefficient may exceed the prediction from Equation 1 in the main text, although this was not observed experimentally in the present work.

S9. Pentane Wettability of Copper and Copper Foam

Both the flat copper and the copper foam wick were completely wetted by pentane, shown in the droplet deposition tests in Figures S4 and S5, where the contact angle was zero as the pentane spread across the flat surface and wicked in to the copper foam.

Figure S4. Time-lapse images of a droplet of pentane impinging on a flat copper surface; the contact angle is zero as the droplet completely spreads over the surface.

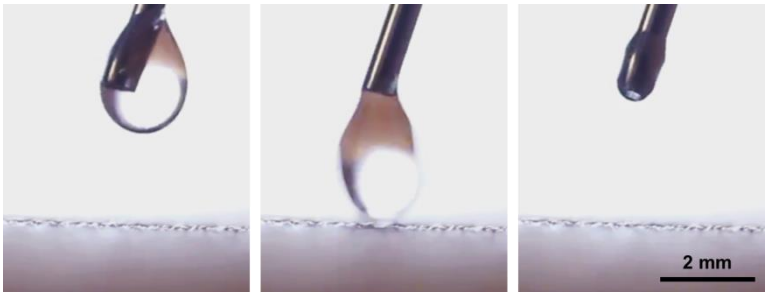

Figure S5. Time-lapse images of a droplet of pentane impinging onto the copper foam; the contact angle is zero as the droplet completely wicks in to the surface.

S10. Non-Dimensionalization of Maximum Heat Transfer Coefficient

Combining Equations 1 and 4 from the main text with the relation for the dimensionless Nusselt Number, Nu = $h_c L/k_L$ (where k_L is the liquid thermal conductivity), we reformulated the maximum possible heat transfer coefficient with a gravitationally-driven wicking condenser into a dimensionless form to facilitate comparisons with literature:

$$Nu = \frac{1}{k_L}\left(\frac{\kappa\rho^2 g h_{fg} k_{wick} L}{\Delta T\, \mu}\right)^{1/2} \quad \text{(S21)}$$

Note that the wick thickness in this case is always optimized; the thickness is a function of the other parameters of the system including wick height, subcooling, condensate viscosity, etc.

Supporting Information References

1. Jung, S. M.; Preston, D. J.; Jung, H. Y.; Deng, Z. T.; Wang, E. N.; Kong, J., Porous Cu nanowire aerosponges from one-step assembly and their applications in heat dissipation. *Adv Mater* **2016,** *28* (7), 1413-1419.

2. (a) Schrader, M. E., Ultrahigh-Vacuum Techniques in Measurement of Contact Angles .3. Water on Copper and Silver. *J Phys Chem-Us* **1974,** *78* (1), 87-89; (b) Preston, D. J.; Mafra, D. L.; Miljkovic, N.; Kong, J.; Wang, E. N., Scalable graphene coatings for enhanced condensation heat transfer. *Nano Lett* **2015,** *15* (5), 2902-2909.

3. (a) Carey, V. P., *Liquid-vapor phase-change phenomena : an introduction to the thermophysics of vaporization and condensation processes in heat transfer equipment*. 2nd ed.; Taylor and Francis: New York, 2008; p 742; (b) Incropera, F. P., *Introduction to heat transfer*. 5th ed.; Wiley: Hoboken, N.J., 2007; p 901.

4. (a) Ma, X. H.; Zhou, X. D.; Lan, Z.; Li, Y. M.; Zhang, Y., Condensation Heat Transfer Enhancement in the Presence of Non-Condensable Gas Using the Interfacial Effect of Dropwise Condensation. *Int J Heat Mass Tran* **2008,** *51* (7-8), 1728-1737; (b) Rose, J. W., Dropwise condensation theory and experiment: a review. *P I Mech Eng a-J Pow* **2002,** *216* (A2), 115-128.